

Multi-Tongue Frequency Fractal Dynamics in Hodgkin–Huxley Neurons Induced by Temporal Interference Stimulation

Madhurendra Mishra¹, Zhen Qi² and Adarsh Ganesan^{3,4}

¹Department of Physics, Sri Guru Tegh Bahadur Khalsa College, University of Delhi, New Delhi, India 110007*

²Department of Electrical and Computer Engineering, Worcester Polytechnic Institute, Worcester, USA 01609-2280[†]

³Department of Electrical and Electronics Engineering, Birla Institute of Technology and Science, Pilani - Dubai Campus, Dubai International Academic City, Dubai, UAE 345055[‡] and

⁴Department of Mechanical Engineering, Birla Institute of Technology and Science, Pilani - Pilani Campus, Vidya Vihar, Pilani, India 333031

(Dated: January 21, 2026)

We investigate neuronal excitability in the Hodgkin–Huxley model under temporal interference (TI) stimulation in a previously unexplored sub-Hz resonant regime and uncover a striking nonlinear response that we term "multi-tongue frequency fractals". Unlike single-frequency driving, which yields a smooth resonant valley, dual-frequency excitation fragments this response into a hierarchy of sharply modulated tongues whose number and structure grow with observation time, revealing clear self-similar architecture. These features emerge from transitions between non-cascaded and cascaded high-harmonic and sub-harmonic generation as detuning varies, and are maximized near the intrinsic ionic timescale at $\omega \approx 0.2$ rad/s. Parameter sweeps show that the fractal count is higher for higher potassium conductances, lower sodium conductances and lower leak conductances. These results demonstrate that TI stimulation can elicit rich, hierarchically organized frequency responses even in classical excitable membranes, revealing fractal organization in Hodgkin–Huxley dynamics.

Introduction— Excitability is a universal dynamical phenomenon observed in a wide class of nonlinear systems, wherein perturbations exceeding a well-defined threshold elicit large, transient responses before the system relaxes back to a stable resting state. Originally identified in biological contexts, excitability has since emerged as a unifying concept across physics, chemistry, and engineering, providing a compact framework for understanding threshold dynamics, pulse generation, and nonlinear signal processing [1, 2].

From a dynamical systems perspective, excitability typically arises near bifurcation points—such as saddle-node or Hopf bifurcations—where slow-fast time-scale separation plays a crucial role. In such regimes, trajectories may undergo large excursions in phase space despite the absence of sustained oscillations, a behavior that has been extensively studied in electronic circuits, optical cavities, chemical reactions, and mechanical resonators [3, 4]. These physical realizations highlight that excitability is not restricted to living systems but is instead a generic consequence of nonlinear feedback and thresholded instability.

The canonical theoretical description of excitability in neuroscience is provided by the Hodgkin–Huxley (HH) model, which describes the action potential as a nonlinear dynamical response of the neuronal membrane driven by voltage-dependent ion channel kinetics [5–7]. Beyond its biological relevance, the HH model has profoundly in-

fluenced the study of excitable media in physics, inspiring reduced descriptions such as the FitzHugh–Nagumo model and motivating experimental investigations in synthetic and engineered systems [3, 8–11]. These developments established excitability as a paradigmatic nonlinear phenomenon characterized by robustness, reproducibility, and sensitivity to weak stimuli.

In 2017, a significant conceptual advance in the control of excitable systems occurred with the proposal of temporal interference (TI) stimulation by Grossman et al. [12]. The central idea relies on the superposition of two high-frequency electric fields with slightly detuned frequencies, producing a low-frequency envelope capable of selectively modulating neural excitability without directly stimulating superficial tissue. Although individual carrier frequencies lie beyond the neuronal firing bandwidth, their interference generates an effective modulation that can cross excitability thresholds in targeted regions.

Subsequent experimental and theoretical studies demonstrated that temporal interference can induce spiking, modulate firing rates, and achieve spatially selective deep-brain stimulation, thereby revealing a new route for noninvasive control of excitable dynamics [13, 14]. From a nonlinear dynamics standpoint, TI stimulation exploits the intrinsic threshold structure of excitable systems, effectively reshaping the input landscape without altering the underlying resting state.

Despite growing experimental support, the mechanisms underlying temporal interference stimulation were investigated only recently based on Hodgkin–Huxley dynamics [15–17]. These studies showed that high-frequency sinusoidal stimulation drives neurons into a

* Email: madhurendramishra24@gmail.com

† Email: zqi@wpi.edu

‡ Email: adarsh@dubai.bits-pilani.ac.in

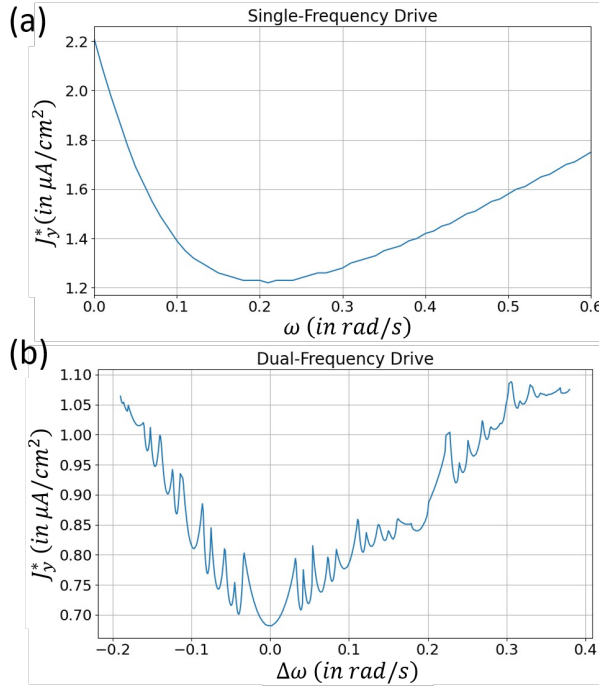


FIG. 1. Stimulation threshold amplitude J_y^* under (a) single-frequency and (b) dual-frequency excitation. In (a), J_y^* reaches its minimum near $\omega \approx 0.2$ rad/s. In (b), the dual-frequency drive produces a broader response exhibiting multiple minima of J_y^* corresponding to "multitongue fractals".

stable subthreshold periodic state maintained by a cycle-averaged balance between inward sodium and outward potassium currents.

While the temporal interference stimulation is generally constrained to frequencies in kHz range, we chose frequency in sub-Hz range allowing resonant excitation of Hodgkin-Huxley dynamics similar to [18, 19]. By doing so, we reveal a new dynamical phenomenon which we term here as "multitongue frequency fractal".

The Hodgkin-Huxley (HH) model describes the electrical activity of a neuron by representing the cell membrane as an electrical circuit composed of a capacitor and nonlinear ionic conductors [7, 20]. The membrane dynamics are governed by the following set of coupled differential equations:

$$C_m \frac{dV}{dt} = I_{\text{ext}} - \left[\bar{g}_{\text{Na}} m^3 h (V - V_{\text{Na}}) + \bar{g}_{\text{K}} n^4 (V - V_{\text{K}}) + g_L (V - V_L) \right] \quad (1)$$

Here, V denotes the membrane potential, C_m is the membrane capacitance per unit area, I_{ext} represents the externally applied current, \bar{g}_{Na} is the sodium conductance, V_{Na} is the sodium equilibrium potential, \bar{g}_{K} is the potassium conductance, V_{K} is the potassium equilibrium potential, g_L is the leak conductance and V_L is the leak reversal potential.

The dynamics of the gating variables m , h , and n are governed by first-order kinetics:

$$\begin{aligned} \frac{dm}{dt} &= \varphi [\alpha_m(V)(1 - m) - \beta_m(V)m] \\ \frac{dh}{dt} &= \varphi [\alpha_h(V)(1 - h) - \beta_h(V)h] \\ \frac{dn}{dt} &= \varphi [\alpha_n(V)(1 - n) - \beta_n(V)n] \end{aligned} \quad (2)$$

Each gating variable represents the probability that a specific channel gate is open. The functions $\alpha_x(V)$ and $\beta_x(V)$ denote voltage-dependent opening and closing rates, respectively.

The rate constants are defined as follows:

$$\begin{aligned} \alpha_m(V) &= \frac{0.1(25 - V)}{\exp\left(\frac{25 - V}{10}\right) - 1} \\ \beta_m(V) &= 4 \exp\left(-\frac{V}{18}\right) \\ \alpha_h(V) &= 0.07 \exp\left(-\frac{V}{20}\right) \\ \beta_h(V) &= \frac{1}{\exp\left(-\frac{V+30}{10}\right) + 1} \\ \alpha_n(V) &= \frac{0.01(10 - V)}{\exp\left(\frac{10 - V}{10}\right) - 1} \\ \beta_n(V) &= 0.125 \exp\left(-\frac{V}{80}\right) \end{aligned}$$

These expressions are empirically derived to fit voltage-clamp experimental data and capture the nonlinear voltage dependence of ion channel kinetics [7].

The parameter φ accounts for temperature-dependent changes in channel kinetics and is defined as $\varphi = 3^{\frac{T-6.3}{10}}$. Here, the temperature T is set to 6.3°C, yielding $\varphi = 1$, to avoid temperature effects on neuronal electrical activity.

We numerically investigate neuronal excitability under temporal interference (TI) stimulation using a single-compartment Hodgkin-Huxley (HH) neuron model. The parameter values are set as $C_m = 1 \mu\text{F}/\text{cm}^2$, $g_K = 36 \text{ mS}/\text{cm}^2$, $g_L = 0.3 \text{ mS}/\text{cm}^2$ and $g_{\text{Na}} = 120 \text{ mS}/\text{cm}^2$, with potentials $V_{\text{Na}} = 115 \text{ mV}$, $V_{\text{K}} = -12 \text{ mV}$ and $V_L = 10.59 \text{ mV}$. To set the resting membrane potential to zero, the membrane voltage is shifted by 65 mV. The initial conditions are set as $V(0) = 0$, $m(0) = 0.053$, $h(0) = 0.596$, $n(0) = 0.317$. These values correspond to the steady-state resting conditions of the HH neuron model.

The temporal interference stimulation current I_{ext} is defined as

$$I_{\text{ext}}(t) = J_y \left[\sin(\omega t) + \sin((\omega + \Delta\omega)t) + 1 \right] \quad (3)$$

where J_y is the stimulation amplitude, ω is the carrier angular frequency, and $\Delta\omega$ is the detuning. Throughout

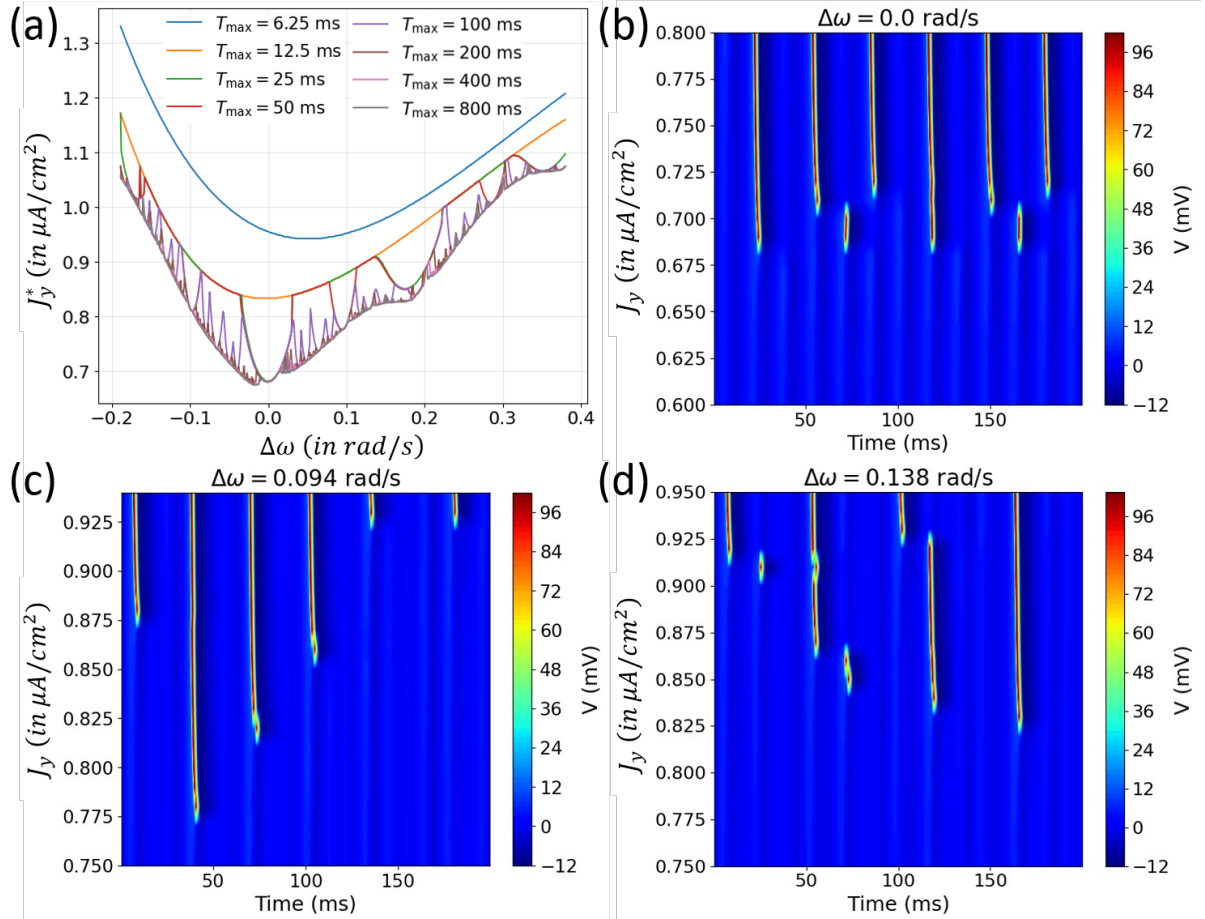


FIG. 2. (a) Stimulation threshold amplitude J_y^* under dual-frequency excitation for different maximum integration times T_{\max} , showing the emergence of tongues within valleys like fractals as the observation window increases. As T_{\max} increases, additional tongue-like substructures appear within the primary valleys, producing a self-similar, fractal-like frequency response. Panels (b)-(d) illustrate three representative contrasting dynamical behaviors responsible for this structure: (b) non-cascaded high-harmonic excitation at $\Delta\omega = 0$, (c) cascaded high-harmonic excitation at $\Delta\omega \approx 0.094$ rad/s, and (d) cascaded subharmonic excitation at $\Delta\omega \approx 0.138$ rad/s. The coexistence and transition among these distinct response regimes collectively generate the hierarchical “frequency fractals” observed in (a).

the simulations, the carrier frequency is fixed at $\omega = 0.2$, while $\Delta\omega$ is systematically varied, enforcing a clear separation of timescales which is required for effective TI stimulation. Owing to the intrinsic low-pass filtering properties of neuronal membranes, the neuron is largely insensitive to the high-frequency carrier and responds primarily to the slow envelope modulation.

Spike initiation is defined by a membrane potential crossing a fixed threshold, $V(t) > V_{\text{th}} = 50$ mV. The HH equations are integrated forward in time, and the minimum stimulation amplitude J_y required to elicit at least one spike is determined using a binary search algorithm. This procedure assumes monotonicity of spike initiation with respect to stimulation amplitude and yields the firing threshold function J_y^* .

As we observe, Fig. 1 establishes the fundamental contrast between single- and dual-frequency stimulation of the Hodgkin–Huxley membrane. Under single-frequency

driving, the stimulation threshold amplitude J_y^* varies smoothly with frequency and exhibits a shallow minimum near the intrinsic resonance. However, when a second tone is introduced, this simple valley fragments into a series of sharp lobes and dips i.e “multitongue fractals”. The emergence of these distinct modulation tongues demonstrates strong nonlinear frequency mixing and indicates that the membrane acts as a nonlinear envelope detector that is highly sensitive to the slow beat component generated by temporal interference.

The hierarchical structure of these modulation tongues is revealed in Fig. 2. As the observation window T_{\max} is increased, smooth valleys split into progressively finer tongue-like features, resulting in a self-similar, fractal-like frequency landscape. Representative voltage traces indicate the dynamical origin of this structure: at $\Delta\omega = 0$, the response corresponds to non-cascaded high-harmonic generation wherein all harmonics are excited

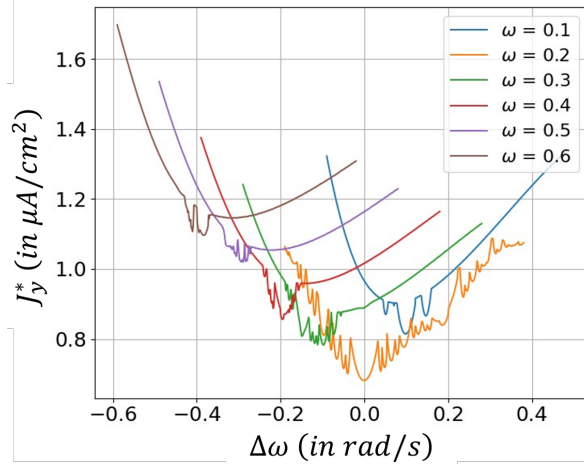


FIG. 3. Stimulation threshold amplitude J_y^* under dual-frequency excitation for different primary drive frequencies ω as a function of detuning $\Delta\omega$. A fractal-like modulation of the response is most prominently observed near the resonant condition at $\omega = 0.2$ rad/s, where the system displays the widest spread and highest complexity of oscillatory structures. As ω increases away from resonance, these frequency-fractal features become confined to a progressively narrower detuning range and their intensity is significantly reduced, leading to smoother response curves.

simultaneously above $J_y \approx 0.68\mu A/cm^2$; at intermediate detuning ($\Delta\omega \approx 0.094$ rad/s), the system exhibits cascaded high-harmonic generation wherein the fundamental tone is excited first and the higher order harmonics are subsequently excited at higher J_y values; at larger detuning ($\Delta\omega \approx 0.138$ rad/s), cascaded sub-harmonic excitation is observed wherein the subharmonics are generated as J_y is increased. The coexistence of these qualitatively distinct regimes, along with sharp transitions among them as detuning varies, generates the observed "multitongue frequency fractals".

Fig. 3 demonstrates that this phenomenon is resonantly organized. When the primary driving frequency is tuned near $\omega = 0.2$ rad/s, the tongues are the most numerous, extend over the widest detuning range, and display the highest amplitude, indicating maximal nonlinear mixing. As the carrier frequency moves away from resonance, the fractal structures compress and the response gradually smoothens. This shows that the multifractal behaviour is not incidental, but is resonantly amplified when the temporal interference envelope matches the intrinsic ionic time scales.

To determine the ionic mechanisms responsible for these dynamics, we independently varied the sodium, potassium, and leak conductances as shown in Fig. 4. Increasing g_{Na} significantly enhances excitability leading to lower stimulation threshold J_y^* . In contrast, higher g_K values correspond to higher J_y^* values. Increasing the leak conductance g_L suppresses high-frequency structure and smoothens the response. These effects are quantified in Fig. 5, which maps fractal counts across the (g_{Na}, g_K)

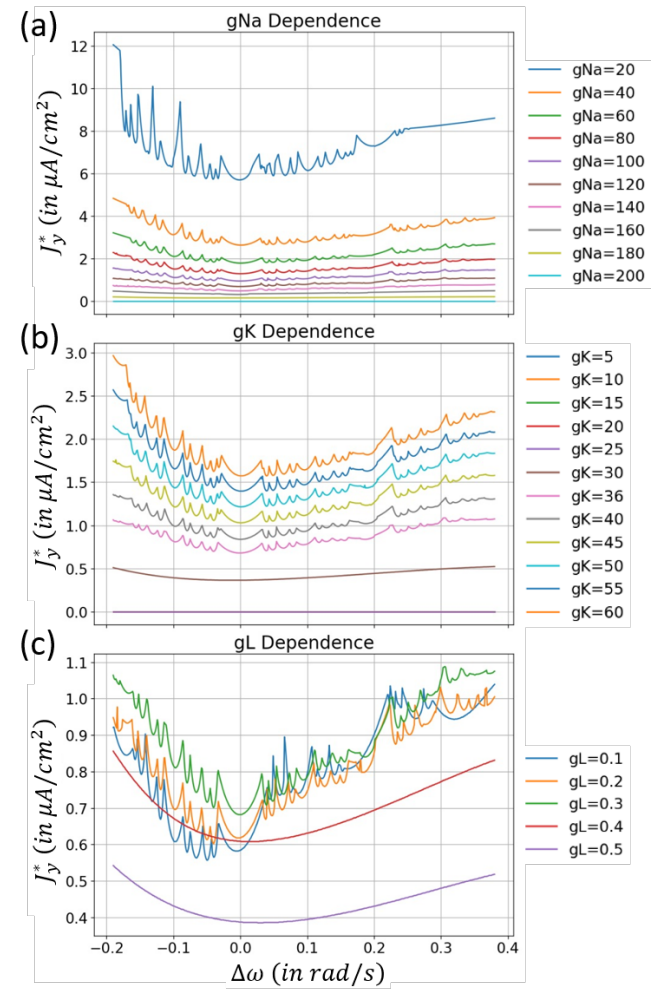


FIG. 4. (a-c) Effect of Hodgkin–Huxley model parameters viz. g_{Na} , g_K and g_L on the dual-frequency response respectively. Although higher g_{Na} , lower g_K and higher g_L promote excitability, they do not favor the formation of multitongue frequency fractals.

parameter space for different g_L values. For low leak conductance, a broad region supports high fractal counts. As g_L increases, this region contracts and shifts toward higher g_K and lower g_{Na} , and eventually most of the parameter space becomes dynamically regular. This reveals a clear transition from a strongly nonlinear, multifractal regime to a leak-dominated quasi-linear regime, establishing the frequency-fractal response as a distinct and controllable dynamical phase of the Hodgkin–Huxley model.

Conclusions— In this work, we demonstrate that temporal interference stimulation fundamentally reorganizes the excitability landscape of the Hodgkin–Huxley neuron, giving rise to the phenomenon of 'multitongue frequency fractals'. Unlike the smooth single-frequency response, dual-frequency drive fragments the excitability profile into hierarchically structured lobes and dips

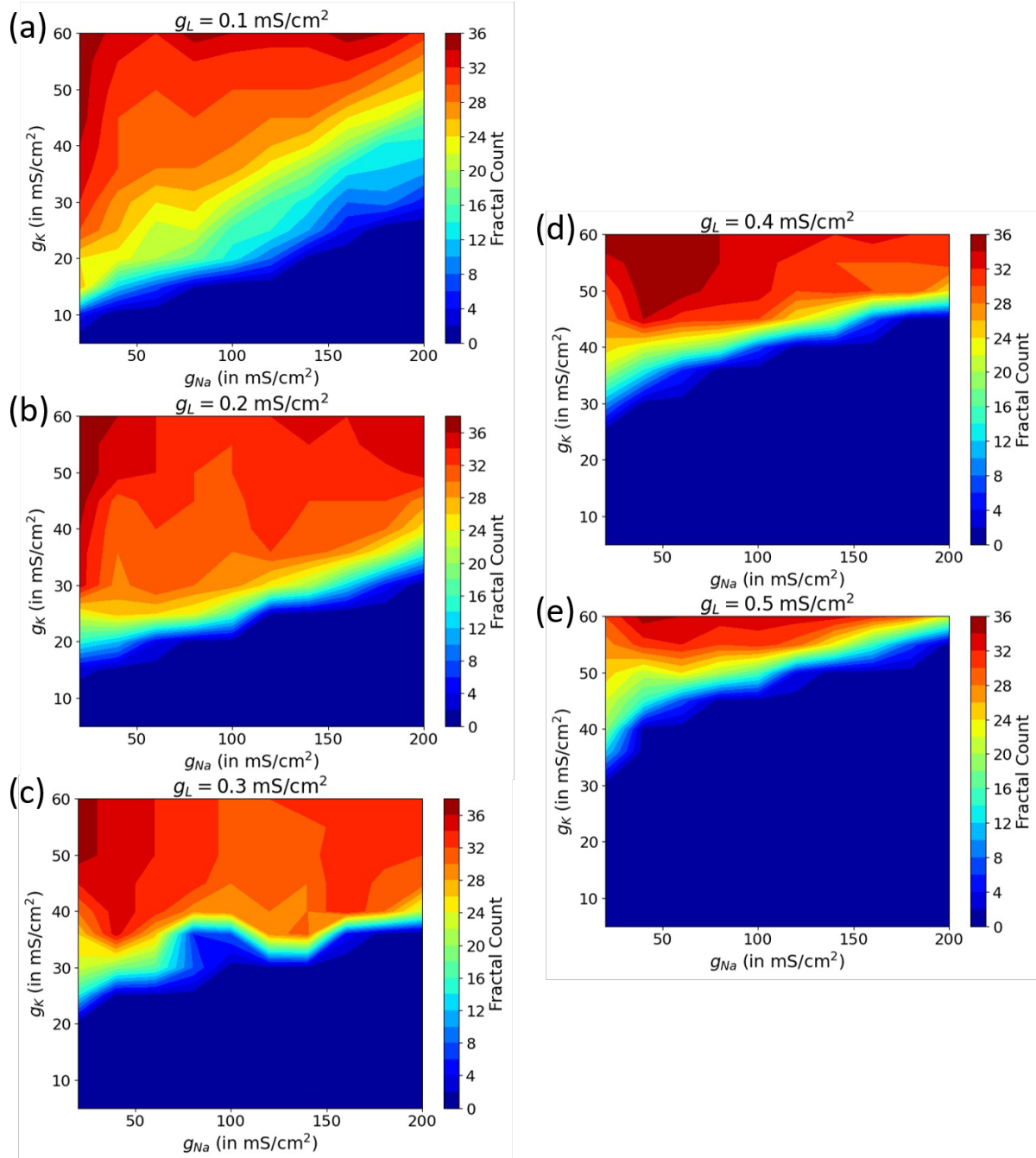


FIG. 5. Fractal count maps showing how the sodium conductance g_{Na} and potassium conductance g_{K} together determine the strength of multifractal behaviour for different values of leak conductance g_{L} . Panels (a)–(e) correspond to increasing g_{L} from 0.1 to 0.5 mS/cm^2 . For low g_{L} , a large region of the $(g_{\text{Na}}, g_{\text{K}})$ space supports high fractal counts, indicating strong nonlinear interactions between sodium excitation and potassium recovery currents. As g_{L} increases, this high-fractal region gradually shrinks and shifts toward higher g_{K} and lower g_{Na} , and most of the parameter space eventually becomes non-fractal (dark-blue region).

that refine with increasing observation time, revealing clear self-similar structure. This structure arises from the coexistence of non-cascaded high-harmonic generation, cascaded high-harmonic generation and cascaded sub-harmonic generation, and from the sharp

switching between these regimes as detuning varies. The phenomenon is resonantly organized, becoming most pronounced when the carrier frequency aligns with intrinsic ionic timescales, thereby maximizing nonlinear envelope interactions. Systematic conductance tuning

shows that ionic parameters influence the fractal count demonstrating "multitongue frequency fractal" as a dis-

tinct, tunable dynamical phase of the Hodgkin-Huxley neuron.

[1] E. M. Izhikevich, *Dynamical Systems in Neuroscience: The Geometry of Excitability and Bursting* (MIT Press, Cambridge, MA, 2007).

[2] A. Pikovsky, M. Rosenblum, and J. Kurths, *Synchronization: A Universal Concept in Nonlinear Sciences* (Cambridge University Press, Cambridge, 2001).

[3] R. FitzHugh, Impulses and physiological states in theoretical models of nerve membrane, *Biophysical Journal* **1**, 445 (1961).

[4] E. Meron, Pattern formation in excitable media, *Physics Reports* **218**, 1 (1992).

[5] A. L. Hodgkin and A. F. Huxley, A quantitative description of membrane current and its application to conduction and excitation in nerve, *The Journal of Physiology* **117**, 500 (1952).

[6] M. Nelson and J. Rinzel, The hodgkin—huxley model, in *The book of GENESIS: exploring realistic neural models with the GEneral NEural SImulation System* (Springer, 1998) pp. 29–49.

[7] Y. Yuan, Y. Chen, and X. Li, Theoretical analysis of transcranial magneto-acoustical stimulation with hodgkin-huxley neuron model, *Frontiers in Computational Neuroscience* **10**, 35 (2016).

[8] T. Levi, F. Khoyratee, S. Saighi, and Y. Ikeuchi, Digital implementation of hodgkin–huxley neuron model for neurological diseases studies, *Artificial Life and Robotics* **23**, 10 (2018).

[9] G. H. Rutherford, Z. D. Mobile, J. Brandt-Trainer, R. Follmann, and E. Rosa, Analog implementation of a hodgkin–huxley model neuron, *American Journal of Physics* **88**, 918 (2020).

[10] J. Kumar, J. Kumar, S. Murali, and R. Bhakthavatchalu, Design and implementation of izhikevich, hodgkin and huxley spiking neuron models and their comparison, in *2016 International Conference on Advanced Communication Control and Computing Technologies (ICACCCT)* (IEEE, 2016) pp. 111–116.

[11] A. G. Giannari and A. Astolfi, Model design for networks of heterogeneous hodgkin–huxley neurons, *Neurocomputing* **496**, 147 (2022).

[12] N. Grossman, D. Bono, N. Dedic, S. H. Kodandaramiah, A. Rudenko, H. J. Suk, A. M. Cassara, E. Neufeld, N. Küster, L.-H. Tsai, A. Pascual-Leone, and E. S. Boyden, Noninvasive deep brain stimulation via temporally interfering electric fields, *Cell* **169**, 1029 (2017).

[13] E. Mirzakhalili, B. Barra, M. Capogrosso, and S. F. Lempka, Biophysics of temporal interference stimulation, *Cell Systems* **11**, 557 (2020).

[14] Z. Esmaeilpour, G. Kronberg, D. Reato, L. C. Parra, and M. Bikson, Temporal interference stimulation targets deep brain regions by modulating neural oscillations, *Brain Stimulation* **14**, 55 (2021).

[15] T. Plovie, R. Schoeters, T. Tarnaud, L. Martens, W. Joseph, and E. Tanghe, Influence of temporal interference stimulation parameters on point neuron excitability, in *2022 44th Annual International Conference of the IEEE Engineering in Medicine & Biology Society (EMBC)* (IEEE, 2022) pp. 2365–2368.

[16] T. Plovie, R. Schoeters, T. Tarnaud, W. Joseph, and E. Tanghe, Contribution of ion channel nonlinearities to the mechanism of temporal interference stimulation, in *The 3rd Annual Conference of BioEM (BioEM 2024)* (2024) pp. 1–8.

[17] T. Plovie, R. Schoeters, T. Tarnaud, W. Joseph, and E. Tanghe, Nonlinearities and timescales in neural models of temporal interference stimulation, *Bioelectromagnetics* **46**, e22522 (2025).

[18] P. Parmananda, H. Mahara, T. Amemiya, and T. Yamaguchi, Resonance induced pacemakers: A new class of organizing centers for wave propagation in excitable media, *Physical review letters* **87**, 238302 (2001).

[19] P. Parmananda, C. H. Mena, and G. Baier, Resonant forcing of a silent hodgkin-huxley neuron, *Physical Review E* **66**, 047202 (2002).

[20] M. G. Johnson and S. Chartier, Spike neural models (part i): The hodgkin-huxley model, *The quantitative methods for psychology* **13**, 105 (2017).